JACS
JOURNAL OF THE AMERICAN CHEMICAL SOCIETY
pubs.acs.org/JACS
Article

Triply Bonded Pancake π-Dimers Stabilized by Tetravalent Actinides

Luciano Barluzzi,* Sean P. Ogilvie, Alan B. Dalton, Peter Kaden, Robert Gericke, Akseli Mansikkamäki,* Sean R. Giblin, and Richard A. Layfield*

Cite This: J. Am. Chem. Soc. 2024, 146, 4234−4241

Read Online

ACCESS | Metrics & More | Article Recommendations | Supporting Information

ABSTRACT: Aromatic π-stacking is a weakly attractive, noncovalent interaction often found in biological macromolecules and synthetic supramolecular chemistry. The weak nondirectional nature of π-stacking can present challenges in the design of materials owing to their weak, nondirectional nature. However, when aromatic π-systems contain an unpaired electron, stronger attraction involving face-to-face π-orbital overlap is possible, resulting in covalent so-called "pancake" bonds. Two-electron, multicenter single pancake bonds are well known, whereas four-electron double pancake bonds are rare. Higher-order pancake bonds have been predicted, but experimental systems are unknown. Here, we show that six-electron triple pancake bonds can be synthesized by a 3-fold reduction of hexaazatrinaphthylene (HAN) and subsequent stacking of the $[HAN]^{3-}$ triradicals. Our analysis reveals a multicenter covalent triple pancake bond consisting of a σ-orbital and two equivalent π-orbitals. An electrostatic stabilizing role is established for the tetravalent thorium and uranium ions in these systems. We also show that the electronic absorption spectrum of the triple pancake bonds closely matches computational predictions, providing experimental verification of these unique interactions. The discovery of conductivity in thin films of triply bonded π-dimers presents new opportunities for the discovery of single-component molecular conductors and other spin-based molecular materials.

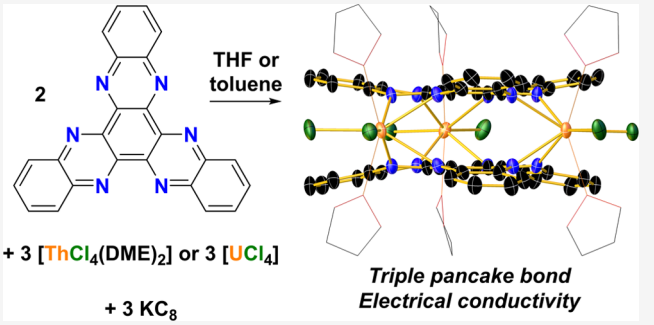

INTRODUCTION

Attractive noncovalent interactions between π-electron clouds play vital roles in structural biology, drug binding[1,2] and in the assembly of supramolecular materials.[3−5] A different, stronger form of attraction between π-systems containing radical electrons can also occur, whereby multicenter intermolecular π-overlap leads to cofacial interactions referred to as "pancake" bonds.[6] Pancake bonds form through covalent overlap of a singly occupied π-molecular orbital (π-SOMO) on one radical with that of another, forming a multicenter two-electron bond and a dimer with a singlet ground state.[7] Pancake dimers display atom−overatom stacking, with molecules separated by distances shorter than the sum of van der Waals radii, in contrast to the slip-stacked structures and longer inter-ring distances found in classical π-stacks.[8−11] Motivation for studying pancake dimers stems from their chemically modifiable electronic structure, which shows potential for applications in conducting organic materials and in materials for quantum information processing.[12−14]

Following early studies demonstrating the electrical conductivity properties of organic π-dimers,[15−17] attention continues to focus on pancake bonds formed through dimerization of neutral phenalenyl (PLY) radicals.[18−24] The prototypical dimer $(PLY)_2$ illustrates how SOMO−SOMO overlap results in an atom−over−atom structure and a pancake bond order of one (Scheme 1).[20]

Scheme 1. Upper: Dimerization of PLY Radicals to Give $(PLY)_2$ via Cofacial π-Orbital Overlap; Lower: Simplified Molecular Orbital Scheme for $(PLY)_2$

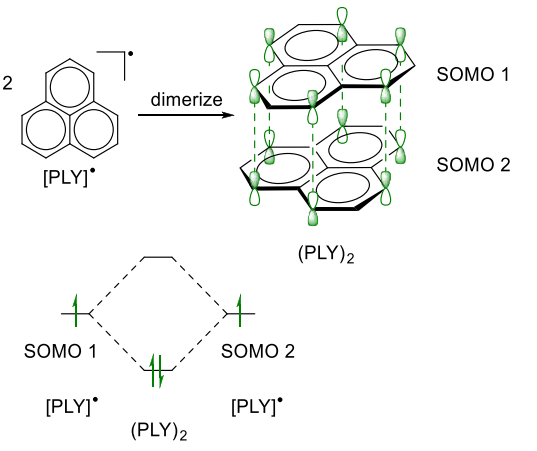

Received: December 9, 2023
Revised: January 22, 2024
Accepted: January 23, 2024
Published: February 6, 2024

https://doi.org/10.1021/jacs.3c13914
J. Am. Chem. Soc. 2024, 146, 4234−4241

Pancake single bonds have also been observed in dimers of electron-deficient organic compounds[25−27] and they are frequently found in the solid-state structures of sulfur−nitrogen heterocycles.[6,28−30] Double pancake bonds form via π-systems consisting of two unpaired electrons, as proposed for the hypothetical dimer of dithiatriazine rings $(S_2N_3CH)_2$, thus explaining the small inter-ring separation in the experimental system $(S_2N_3CPh)_2$.[28,29,31] Despite challenges to the double pancake bond description,[32] further evidence in support of such interactions has emerged.[33] Double pancake bonding in hypothetical boron- and nitrogen-doped $(PLY)_2$ dimers has also been proposed,[34] and computational modeling of stacked dimeric triangulene graphene flakes predicts that pancake bond orders up to five might be achievable with multiradical monomers.[35]

Although pancake dimers with bond orders greater than two are unknown, the isolation of higher-order pancake bonds is a key target that would aid the validation of theoretical models while also providing new opportunities for the discovery of spin-based functional molecular materials. We now report the synthesis of triple pancake bonds based on the triradical trianion derived from the extended aromatic system hexaazatrinaphthylene, i.e., $[HAN]^{3-}$.

RESULTS AND DISCUSSION

To achieve effective cofacial overlap of π-orbitals in two $[HAN]^{3-}$ anions, mitigation of Coulombic repulsions between the monomers is required. We selected the tetravalent actinides thorium(IV) and uranium(IV) for this purpose, whose large radii, high formal oxidation state, and affinity for nitrogen-donor ligands should stabilize the interaction. The target compounds $[\{MCl_2(THF)_2\}_3(HAN)_2]$ (M = Th, **1-Th**; M = U, **1-U**) were synthesized by the reduction of HAN with potassium graphite (KC_8) in the presence of the actinide(IV) precursors $[ThCl_4(DME)_2]$ and UCl_4 (Scheme 2, DME = 1,2-dimethoxyethane).

Scheme 2. Synthesis of 1-Th (M = Th) and 1-U (M = U) from the Reaction of HAN with Thorium(IV) or Uranium(IV) Chloride and Potassium Graphite

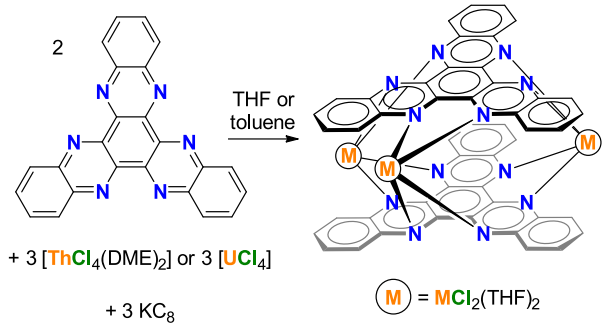

Compound **1-Th** crystallizes in trigonal space group $R\bar{3}$ with half a molecule of benzene per formula unit, and **1-U** crystallizes in monoclinic space group $P2_1/m$ (Table S1). Compounds **1-Th** and **1-U** have similar structures (Figures 1, S1−S3), consisting of three eight-coordinate actinide(IV) centers occupying distorted triangular dodecahedral geometries (Tables S2 and S3), with two terminal chloride ligands, two THF ligands and two bridging bidentate HAN ligands. In **1-Th**, the Th−O1 and Th−O2 bond distances are 2.571(5) and 2.595(5) Å, respectively, and the Th−Cl1 and

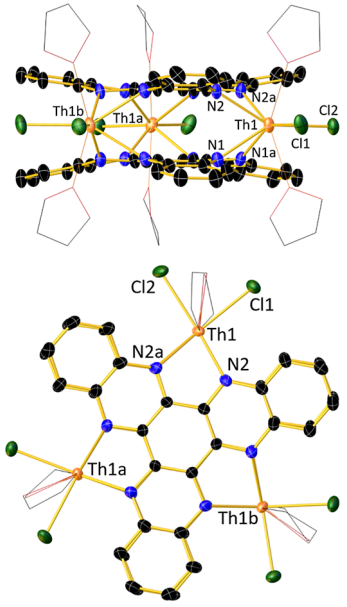

Figure 1. Upper: thermal ellipsoid representation (30% probability) of the molecular structure of **1-Th** viewed along the crystallographic *a*-axis (for clarity, the THF ligands are depicted as wireframes, and hydrogen atoms are omitted). Lower: molecular structure of **1-Th** viewed along the crystallographic *c*-axis.

Th−Cl2 distances are 2.686(2) and 2.693(2) Å, respectively. The Th−N1 and Th−N2 bond distances are 2.526(5) and 2.540(6) Å, respectively. In **1-U**, the average U−O bond distance is 2.58(2) Å, and the average U−Cl bond distance is 2.651(8) Å. The U−N bond distances range from 2.47(2) to 2.50(2) Å.

The concave shape of HAN in **1-Th** and **1-U** is reflected in the dihedral angles of 9.75(3) and 8.74(5)°, respectively, formed between the central and peripheral C_6 rings, a striking feature considering that metal complexes of HAN ligands tend to be flat.[36−40] Furthermore, the 30 atoms within one HAN ligand are eclipsed with those in the other ligand in both compounds. The vertical separations between the central C_6 rings in **1-Th** and **1-U** are 2.86(2) and 2.829(9) Å, respectively, markedly shorter than twice the van der Waals radius of carbon (3.40 Å) and the interlayer distance of 3.35 Å in graphite.[41] Whereas no close intermolecular contacts occur in the crystal lattice of **1-Th** (Figures S4, S5), the outer C_6 rings of the HAN ligands in **1-U** adopt slipped supramolecular π-stacking arrangements parallel to the crystallographic *a*-axis, with C···C distances in the range 3.3−3.5 Å (Figures S6 and S7).

After **1-Th** was dried under reduced pressure, the ^{1}H NMR spectrum in THF-D_8 shows that the benzene molecules of crystallization are removed (Figures S8−S10). The ^{1}H NMR spectrum of **1-Th** displays HAN resonances at chemical shifts associated with diamagnetic aromatic compounds, i.e., $\delta(^1H)$ = 8.44−6.52 ppm. The effective magnetic moment (μ_{eff}) of **1-Th** measured using the Evans NMR method is zero (Figure S11). The ^{1}H NMR spectrum of **1-U** is similar to that of the thorium analog (Figures S12 and S13).

Theoretical Study. The $[HAN]^{3-}$ units in **1-Th** and **1-U** can occur either as a monoradical or a triradical, meaning that single or triple pancake bonding is possible in these compounds. Precisely which interaction occurs in **1-Th** and **1-U** is difficult to predict in advance of the synthesis or even in

https://doi.org/10.1021/jacs.3c13914
J. Am. Chem. Soc. 2024, 146, 4234−4241

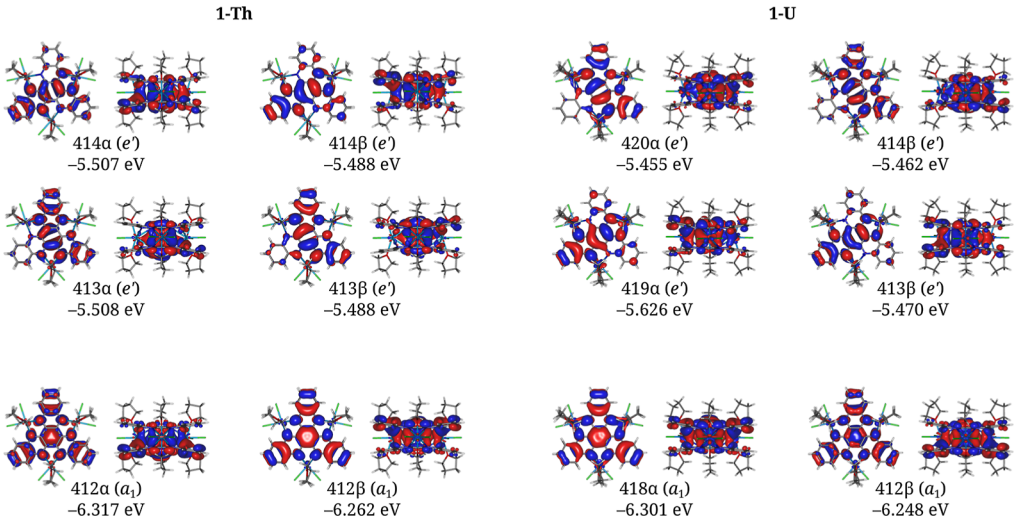

Figure 2. Frontier molecular orbitals in the ground spin states of **1-Th** and **1-U**. Each α- and β-orbital describing the pancake triple bonds in **1-Th** (A) and **1-U** (B) is shown top-down and side-on. Symmetry labels are based on idealized D_{3h} symmetry. The a_1- and e′-symmetric orbitals describe the σ- and two π-components of the pancake bond, respectively.

light of the concave [HAN]···[HAN] interactions found in the solid-state structures. Therefore, we investigated the bonding interactions using density functional theory (DFT) calculations. Both **1-Th** and **1-U** have similar calculated electronic structures, and to simplify the analysis we focused on **1-Th**. The three bonding orbitals between the $[HAN]^{3-}$ radicals in **1-Th** and **1-U** in their ground spin states can be divided into a σ-bonding orbital and two π-bonding orbitals (Figure 2). Under idealized D_{3h} symmetry, the σ-bonding orbital transforms as the totally symmetric A_1 representation and the π-bonding orbital as the E′ representation. The former is the symmetry of a conventional σ-bond, while the latter is the symmetry of a π-bond involving p-orbitals under D_{3h} symmetry.

The bonding was further studied by examining the spin-state energetics using broken-symmetry DFT (Table S4),[42−46] the Yamaguchi projection,[47−49] and the CAM-B3LYP exchange correlation (XC) functional.[50−52] The geometries of the $[HAN]^{3-}$ anions extracted from the crystal structure of **1-Th** have quartet ground states with three unpaired electrons, which are likely stabilized relative to the doublet configuration by the concave structure. The calculated energy difference between the quartet and doublet states is 382 and 712 cm^{-1} for the two radicals. The large difference in energies indicates that the ground spin state of $[HAN]^{3-}$ is sensitive to small distortions, as reported previously.[36] Coupling of three unpaired electrons on free $[HAN]^{3-}$ to form a singlet ground state strongly indicates the formation of a triple bond between the radicals. The radical−radical interaction can be described as antiferromagnetic coupling between the two quartet spins. When the energy differences are described by an isotropic Heisenberg−Dirac−van Vleck Hamiltonian, i.e., $\hat{H}_{HDvV} = -J\hat{S}_A\cdot\hat{S}_B$ with $\hat{S}_A$ and $\hat{S}_B$ denoting effective spin operators on the $[HAN]^{3-}$ radicals, the exchange coupling constants is $J = -2803$ cm^{-1}, indicating a strong antiferromagnetic interaction that is practically a covalent bond. For comparison, the J-value in the dimer of 2,5,8-tri*tert*-butylphenalenyl is in the region of -1300 to -3000 cm^{-1},[53−55] with computational values closer to the lower estimate.[20,22,56] Thus, it is reasonable to classify the interaction between the $[HAN]^{3-}$ anions as a covalent bond.

To further verify that the calculated exchange interaction involves three electrons on both $[HAN]^{3-}$ anions, we also calculated the exchange coupling for a model involving only one unpaired electron on each radical. Here, the exchange coupling is massively strong with $J = -10{,}739$ cm^{-1}. However, the spin expectation value $\langle S^2\rangle$ is 0.973, which for two interacting SOMOs would mean minimal overlap, contradicting the J-value. This result implies that the interaction between the $[HAN]^{3-}$ anions involves six electrons, all of which participate in a covalent interaction, leading to a triple bond.

To obtain a quantitative picture of the bonding energetics in **1-Th**, the molecule was partitioned into fragments and reconstructed in a stepwise manner. Three fragments were chosen: two quartet $[HAN]^{3-}$ anions and a fragment consisting of the three $[ThCl_2(THF)_2]^{2+}$ cations with a total charge of +6. The molecule was constructed from these fragments in two steps by first bonding the $[HAN]^{3-}$ anions to each other and then bonding the resulting $[(HAN)_2]^{6-}$ dimer to the $[ThCl_2(THF)_2]^{2+}$ cations. The energetics of the formation of **1-Th** from the fragments were studied using the Morokuma−Ziegler−Rauk energy decomposition analysis (EDA)[57−59] and the PBE0 XC functional.[60−63] In this approach, the molecular fragments are placed in the same geometry as in the molecule, and the energy associated with formation of the molecule from the fragments is termed the instantaneous interaction energy, ΔE_{inst}. It is related to the bonding energy between the fragments but does not include the energy required to distort the fragments from the optimal geometries to those they possess in the final molecule. The ΔE_{inst} can be partitioned into electrostatic interaction ΔE_{elstat}, orbital interaction ΔE_{orb}, and Pauli repulsion ΔE_{Pauli} terms. The ΔE_{elstat} describes the classic electrostatic interaction between the molecular fragments before the electron densities mix, ΔE_{orb} describes the energy lowering once the fragment densities mix, and ΔE_{Pauli} describes nonclassical repulsion between the fragment densities due to the antisymmetry of the wave function. In addition, the DFT-D3 dispersion correction ΔE_{disp} can be separated from the other energy components. The orbital interaction energy can be further partitioned into contributions from different irreducible representations of the

https://doi.org/10.1021/jacs.3c13914
J. Am. Chem. Soc. 2024, 146, 4234−4241

molecular point group. Symmetry was only utilized in the study of the bonding between the $[HAN]^{3-}$ fragments and, due to the broken-spin nature of the fragments, the highest point-group symmetry is C_{3v}. The results are given in Table 1.

Table 1. Energy Decomposition Analysis of 1-Th[a]

bonding contribution		step 1	step 2
ΔE_{inst}		1831	−11,369
ΔE_{elstat}		1914	−10,473
ΔE_{orb}	total	−376	−3978
	A_1	−89	
	A_2	−19	
	E	−268	
ΔE_{Pauli}		432	3385
ΔE_{disp}		−138	−303

[a]Energies are stated in kJ mol^{-1}. Step 1 describes the interaction between two $[HAN]^{3-}$ quartet radicals to give $[(HAN)_2]^{6-}$. Step 2 describes reconstruction of **1-Th** through the interaction of $[(HAN)_2]^{6-}$ with three $[ThCl_2(THF)_2]^{2+}$ cations.

The EDA shows that the dominant interaction holding **1-Th** together is the electrostatic interaction between the $[HAN]^{3-}$ and $[ThCl_2(THF)_2]^{2+}$ fragments. Orbital interactions and dispersion make smaller but significant bonding contributions to the overall stability. The interaction between the $[HAN]^{3-}$ anions is electrostatically strongly repulsive due to the large negative charges on the two radicals. The bonding orbital interaction describing the covalency, i.e., the pancake bonding, between the $[HAN]^{3-}$ anions is smaller than the electrostatic repulsion but still very significant. This covalent interaction can be further divided into contributions from σ-bonding (A_1 symmetry), π-bonding (E symmetry), and a minor component with A_2 symmetry. Surprisingly, the π bonds appear to be the dominant covalent interaction between the $[HAN]^{3-}$ anions, and the σ bond is about three times weaker. While the EDA results clearly support the existence of the triple pancake bond between $[HAN]^{3-}$ anions, in terms of the overall bonding interactions in **1-Th** the pancake bond is supported by strong electrostatic and orbital (i.e., metal ligand covalency) interactions with the $[ThCl_2(THF)_2]^{2+}$ cations.

Magnetic Properties and Electrical Conductivity. In THF at 300 K, the X-band EPR spectrum of **1-Th** is featureless, confirming diamagnetic behavior (Figure S14). Although **1-U** is paramagnetic by virtue of the $5f^2$ electron configuration of uranium(IV), complexes of this species are typically EPR silent, hence the absence of an EPR signal for **1-U** is consistent with a diamagnetic $[(HAN)_2]^{6-}$ core (Figure S15). The electronic absorption spectra of **1-Th** and **1-U** in the UV/vis/NIR region in THF differ from those reported for complexes containing a single $[HAN]^{3-}$ ligand.[36] Two major absorptions occur for **1-Th** at wavelengths of 360 and 528 nm (Figure S16), which were assigned using time-dependent DFT (TD-DFT) calculations. The observed maximum at 360 nm can be associated with a set of four doubly degenerate pairs of transitions calculated to occur between 320 and 360 nm (Table S6). These transitions correspond to excitations from occupied nonbonding π-orbitals on $[HAN]^{3-}$ and from the pancake bonding orbitals to orbitals that are antibonding with respect to the pancake bond, higher-lying combinations of $[HAN]^{3-}$ π-orbitals, and vacant thorium 6d orbitals. The observed peak at 528 nm is probably related to a single transition predicted by TD-DFT to occur at a wavelength of 469 nm, corresponding to excitation from the pancake bonding orbitals to the pancake antibonding orbitals. Since this transition is directly related to the pancake triple bond, it should correspond to a rough estimate of the strength of the interaction. The UV/vis/NIR spectrum of **1-U** is similar, with

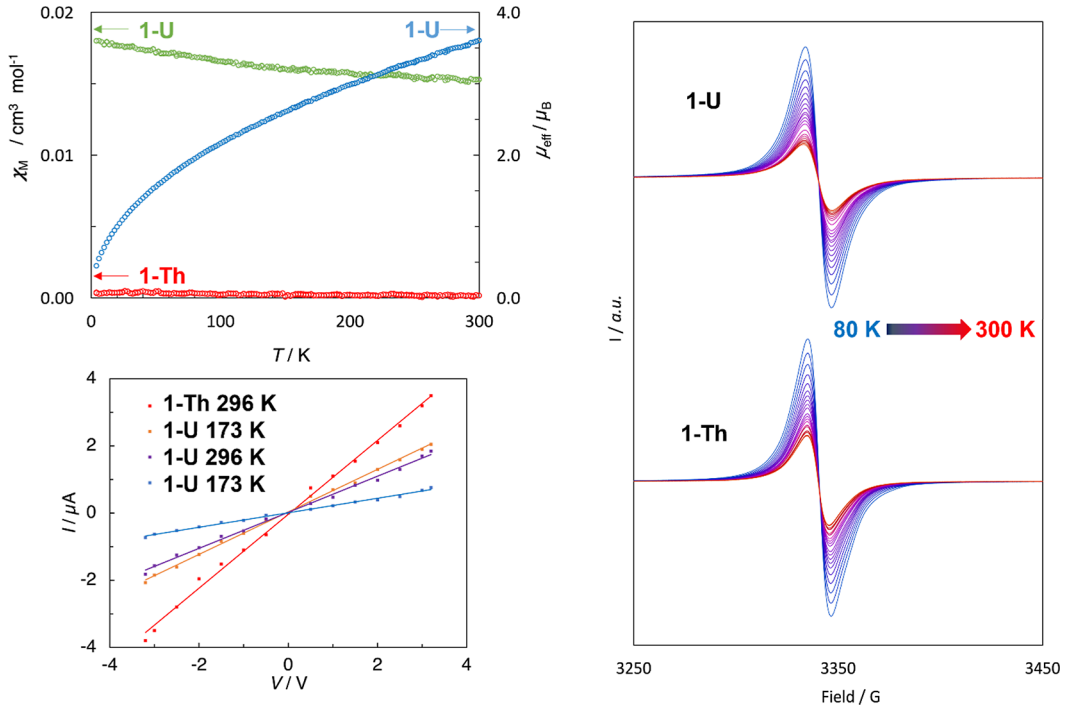

Figure 3. Upper left: molar magnetic susceptibility (χ_M) as a function of temperature for **1-Th** and **1-U**, and effective magnetic moment (μ_{eff}) per uranium(IV) center in **1-U**. Lower left: current−voltage characteristics for drop-cast thin films of **1-Th** and **1-U** at 296 and 173 K. Right: variable-temperature X-band EPR spectra for solid **1-Th** and **1-U** in the range 80−300 K.

https://doi.org/10.1021/jacs.3c13914
J. Am. Chem. Soc. 2024, 146, 4234−4241

absorbances occurring at 326 nm alongside broad absorptions spanning 500−700 nm (Figure S17). The absence of well-defined peaks in the NIR region of the spectrum of **1-U** (Figure S18) is consistent with the presence of uranium(IV).[64]

The temperature dependence of the molar magnetic susceptibility (χ_M) was measured for **1-Th** and **1-U** in the solid state at temperatures in the range of 2−300 K. The susceptibility for **1-U** is typical of uranium(IV),[65] with χ_M increasing slightly from 0.016 $cm^3\ mol^{-1}$ at 300 K to 0.019 $cm^3\ mol^{-1}$ at 2 K, corresponding to μ_{eff} values per uranium(IV) center of 3.61 and 0.45 μ_B, respectively (Figure 3). Compound **1-Th** unexpectedly produced a small, temperature-independent paramagnetic contribution of approximately 2.6×10^{-4} $cm^3\ mol^{-1}$ (Figure 3), reminiscent of the Pauli paramagnetism in electrically conductive solids.[66,67] The X-band EPR spectra of **1-Th** and **1-U** in the solid-state at 300 K displayed a small Lorentzian-shaped resonance centered on *g*-values of 2.0032 and 2.0036 (Figures 3, S19 and S20), respectively, accounting for approximately 2% of the sample (Figures S21−S26 and Supporting Information), and close to the free electron *g*-value. A variable-temperature EPR study at 80−300 K showed that the resonance increases in intensity with decreasing temperature, reminiscent of the conduction electron spin resonance reported for nanostructured graphite[68,69] and graphene.[70,71]

The paramagnetism of the pancake dimers prompted us to investigate their electrical conductivity as thin films, which were prepared by drop-casting THF solutions onto interdigitated gold electrodes (Figures S27−S30). The current (I) was measured at 296 and 173 K using the two-probe technique, with voltages (V) applied at 0.5 V intervals in the range ±3.0 V and at ±3.2 V (Figure 3). Both **1-Th** and **1-U** display linear Ohmic $I-V$ characteristics. The measured current at a given voltage is lower at 173 K. After cooling, data from repeat measurements on both compounds at 296 K were superimposable on the initial data (Figures S31 and S32). The conductivity (σ) of each material at 296 K was calculated using the resistance obtained from the $I-V$ measurements, considering the thickness of the films, the electrode channel length, and the serpentine length along the interdigitated fingers. Values of $\sigma = 1.72 \times 10^{-4}$ and 0.47×10^{-4} S m^{-1} were determined for **1-Th** and **1-U**, respectively, similar to the conductivity reported for solution-processed semiconductor networks.[72]

The electrical conductivity of **1-Th** and **1-U** allows them to be described as single-component molecular conductors, a type of material in which charge transport often relies on noncovalent intermolecular interactions.[73,74] For **1-U**, a conductivity mechanism is possible in which intermolecular π-stacking of the HAN ligands in the crystal lattice facilitates hopping of charge carriers, implying that nonclassical pancake and classical supramolecular π-stacks are both involved in the conductivity. The absence of intermolecular $\pi-\pi$ stacking interactions in the lattice of **1-Th** suggests that charge carrier mobility proceeds through a different mechanism, although it is conceivable that the removal of the benzene molecules when drying the material under reduced pressure decreases the intermolecular separation, providing a potential conduction pathway.

CONCLUSIONS

In conclusion, the reduction of HAN with KC_8 in the presence of the tetravalent actinide chlorides $[ThCl_4(DME)_2]$ and UCl_4 results in the formation of the metal-stabilized cofacial π-dimers $[\{MCl_2(THF)_2\}_3(HAN)_2]$ (M = Th, **1-Th**; M = U, **1-U**). The concave shape of the extended aromatic systems in **1-Th** and **1-U** and their orientation toward each other, with very short inter-ring separations of 2.86(2) and 2.829(9) Å, respectively, indicate the formation of covalent pancake bonds. DFT calculations reveal the presence of triple pancake bonds consisting of a σ- and two π-components. Agreement between the experimental UV/vis/NIR spectra and TD-DFT calculations support the bonding analysis. The observation of temperature-dependent EPR spectra for the notionally diamagnetic compound **1-Th** and the non-Kramers system **1-U** implied that both compounds are electrical conductors. Conductivity values derived from resistance measurements at 296 K did indeed reveal linear Ohmic $I-V$ responses comparable to those found for solution-processed semiconductor materials. Future work on these pancake-bond materials will explore how substitution of the HAN periphery or extension of the π-conjugation impacts on the conductivity properties.

ASSOCIATED CONTENT

Data Availability Statement

Additional research data supporting this publication are available as Supporting Information at DOI: 10.25377/sussex.23703162.

Supporting Information

The Supporting Information is available free of charge at https://pubs.acs.org/doi/10.1021/jacs.3c13914.

Synthesis, spectroscopic characterization, crystallography details, magnetic measurements, EPR spectroscopy, conductivity measurements, computational details (PDF)

Accession Codes

CCDC 2298029−2298030 contain the supplementary crystallographic data for this paper. These data can be obtained free of charge via www.ccdc.cam.ac.uk/data_request/cif, or by emailing data_request@ccdc.cam.ac.uk, or by contacting The Cambridge Crystallographic Data Centre, 12 Union Road, Cambridge CB2 1EZ, UK; fax: +44 1223 336033.

AUTHOR INFORMATION

Corresponding Authors

Luciano Barluzzi − *Department of Chemistry, School of Life Sciences, University of Sussex, Brighton BN1 9QR, U.K.;* orcid.org/0000-0001-6682-342X; Email: l.barluzzi@sussex.ac.uk

Akseli Mansikkamäki − *NMR Research Unit, University of Oulu, Oulu FI-90014, Finland;* orcid.org/0000-0003-0401-4373; Email: akseli.mansikkamaki@oulu.fi

Richard A. Layfield − *Department of Chemistry, School of Life Sciences, University of Sussex, Brighton BN1 9QR, U.K.;* orcid.org/0000-0002-6020-0309; Email: r.layfield@sussex.ac.uk

Authors

Sean P. Ogilvie − *Department of Physics and Astronomy, School of Mathematical and Physical Sciences, University of Sussex, Brighton BN1 9QR, U.K.;* orcid.org/0000-0002-0433-8186

Alan B. Dalton − *Department of Physics and Astronomy, School of Mathematical and Physical Sciences, University of*

Sussex, Brighton BN1 9QR, U.K.; orcid.org/0000-0001-8043-1377

Peter Kaden − *Institute of Resource Ecology, Helmoltz-Zentrum Dresden-Rossendorf, Dresden 01328, Germany;* orcid.org/0000-0002-9414-2936

Robert Gericke − *Institute of Resource Ecology, Helmoltz-Zentrum Dresden-Rossendorf, Dresden 01328, Germany;* orcid.org/0000-0003-4669-0206

Sean R. Giblin − *School of Physics and Astronomy, Cardiff University, Cardiff CF24 3AA, U.K.*

Complete contact information is available at: https://pubs.acs.org/10.1021/jacs.3c13914

Author Contributions

The manuscript was written through contributions of all authors. All authors have given approval to the final version of the manuscript.

Notes

The authors declare no competing financial interest.

■ ACKNOWLEDGMENTS

The authors thank the EPSRC (grants EP/V003089/1 and EP/V046659/1), the German Federal Ministry of Education and Research (BMBF) (Project 02NUK059B, f-Char), the German Federal Ministry of Environment, Nature Conservation, Nuclear Safety, and Consumer Protection (BMUV) (project 1501667), and the Academy of Finland (grant 332294). We also thank the EPSRC UK National Crystallography Service at the University of Southampton for collecting X-ray crystallographic data on **1-U**.

■ REFERENCES

(1) Bootsma, A. N.; Doney, A. C.; Wheeler, S. E. Predicting the Strength of Stacking Interactions between Heterocycles and Aromatic Amino Acid Side Chains. *J. Am. Chem. Soc.* **2019**, *141*, 11027−11035.

(2) Shao, J.; Kuiper, B. P.; Thunnissen, A.-M. W. H.; Cool, R. H.; Zhou, L.; Huang, C.; Dijkstra, B. W.; Broos, J. The Role of Tryptophan in π Interactions in Proteins: An Experimental Approach. *J. Am. Chem. Soc.* **2022**, *144*, 13815−13822.

(3) Ramakrishnan, R.; Niyas, M. A.; Lijina, M. P.; Hariharan, M. Distinct Crystalline Aromatic Structural Motifs: Identification, Classification, and Implications. *Acc. Chem. Res.* **2019**, *52*, 3075−3086.

(4) Yao, Z.-F.; Wang, J.-Y.; Pei, J. Control of π-π Stacking via Crystal Engineering in Organic Conjugated Small Molecule Crystals. *Cryst. Growth Des.* **2018**, *18*, 7−15.

(5) Li, X.; Ge, W.; Guo, S.; Bai, J.; Hong, W. Characterization and Application of Supramolecular Junctions. *Angew. Chem., Int. Ed.* **2023**, *62*, No. e202216819.

(6) Preuss, K. E. Pancake Bonds: π-Stacked Dimers of Organic and Light-Atom Radicals. *Polyhedron* **2014**, *79*, 1−15.

(7) Kertesz, M. Pancake Bonding: An Unusual Pi-Stacking Interaction. *Chem. Eur. J.* **2019**, *25*, 400−416.

(8) Hunter, C. A.; Sanders, J. K. M. The nature of .pi.-.pi. interactions. *J. Am. Chem. Soc.* **1990**, *112*, 5525−5534.

(9) Herbert, J. M. Neat, Simple, and Wrong: Debunking Electrostatic Fallacies Regarding Noncovalent Interactions. *J. Phys. Chem. A* **2021**, *125*, 7125−7137.

(10) Carter-Fenk, K.; Herbert, J. M. Reinterpreting π-Stacking. *Phys. Chem. Chem. Phys.* **2020**, *22*, 24870−24886.

(11) Martinez, C. R.; Iverson, B. L. Rethinking the Term "Pi-Stacking". *Chem. Sci.* **2012**, *3*, 2191−2201.

(12) Morita, Y.; Suzuki, S.; Sato, K.; Takui, T. Synthetic Organic Spin Chemistry for Structurally Well-Defined Open-Shell Graphene Fragments. *Nat. Chem.* **2011**, *3*, 197−204.

(13) Raman, K. V.; Kamerbeek, A. M.; Mukherjee, A.; Atodiresei, N.; Sen, T. K.; Lazić, P.; Caciuc, V.; Michel, R.; Stalke, D.; Mandal, S. K.; Blügel, S.; Münzenberg, M.; Moodera, J. S. Interface-Engineered Templates for Molecular Spin Memory Devices. *Nature* **2013**, *493*, 509−513.

(14) Lemes, M. A.; Mavragani, N.; Richardson, P.; Zhang, Y.; Gabidullin, B.; Brusso, J. L.; Moilanen, J. O.; Murugesu, M. Unprecedented Intramolecular Pancake Bonding in a Dy_2 Single-Molecule Magnet. *Inorg. Chem. Front.* **2020**, *7*, 2592−2601.

(15) Itkis, M. E.; Chi, X.; Cordes, A. W.; Haddon, R. C. Magneto-Opto-Electronic Bistability in a Phenalenyl-Based Neutral Radical. *Science* **2002**, *296*, 1443−1445.

(16) Pal, S. K.; Itkis, M. E.; Tham, F. S.; Reed, R. W.; Oakley, R. T.; Haddon, R. C. Resonating Valence-Bond Ground State in a Phenalenyl-Based Neutral Radical Conductor. *Science* **2005**, *309*, 281−284.

(17) Bag, P.; Itkis, M. E.; Pal, S. K.; Bekyarova, E.; Donnadieu, B.; Haddon, R. C. Synthesis, Structure and Solid State Properties of Benzannulated Phenalenyl Based Neutral Radical Conductor. *J. Phys. Org. Chem.* **2012**, *25*, 566−573.

(18) Cui, Z.; Gupta, A.; Lischka, H.; Kertesz, M. Concave or Convex π-Dimers: The Role of the Pancake Bond in Substituted Phenalenyl Radical Dimers. *Phys. Chem. Chem. Phys.* **2015**, *17*, 23963−23969.

(19) Mou, Z.; Uchida, K.; Kubo, T.; Kertesz, M. Evidence of σ- and π-Dimerization in a Series of Phenalenyls. *J. Am. Chem. Soc.* **2014**, *136*, 18009−18022.

(20) Suzuki, S.; Morita, Y.; Fukui, K.; Sato, K.; Shiomi, D.; Takui, T.; Nakasuji, K. Aromaticity on the Pancake-Bonded Dimer of Neutral Phenalenyl Radical as Studied by MS and NMR Spectroscopies and NICS Analysis. *J. Am. Chem. Soc.* **2006**, *128*, 2530−2531.

(21) Zhong, R.-L.; Gao, F.-W.; Xu, H.-L.; Su, Z.-M. Strong Pancake 2e/12c Bond in π-Stacking Phenalenyl Derivatives Avoiding Bond Conversion. *ChemPhysChem* **2019**, *20*, 1879−1884.

(22) Small, D.; Zaitsev, V.; Jung, Y.; Rosokha, S. V.; Head-Gordon, M.; Kochi, J. K. Intermolecular π-to-π Bonding between Stacked Aromatic Dyads. Experimental and Theoretical Binding Energies and Near-IR Optical Transitions for Phenalenyl Radical/Radical versus Radical/Cation Dimerizations. *J. Am. Chem. Soc.* **2004**, *126*, 13850−13858.

(23) Xiang, Q.; Guo, J.; Xu, J.; Ding, S.; Li, Z.; Li, G.; Phan, H.; Gu, Y.; Dang, Y.; Xu, Z.; Gong, Z.; Hu, W.; Zeng, Z.; Wu, J.; Sun, Z. Stable Olympicenyl Radicals and Their π-Dimers. *J. Am. Chem. Soc.* **2020**, *142*, 11022−11031.

(24) Cui, Z.; Wang, M.; Lischka, H.; Kertesz, M. Unexpected Charge Effects Strengthen π-Stacking Pancake Bonding. *JACS Au* **2021**, *1*, 1647−1655.

(25) Mota, F.; Miller, J. S.; Novoa, J. J. Comparative Analysis of the Multicenter, Long Bond in [TCNE]·- and Phenalenyl Radical Dimers: A Unified Description of Multicenter, Long Bonds. *J. Am. Chem. Soc.* **2009**, *131*, 7699−7707.

(26) Garcia-Yoldi, I.; Miller, J. S.; Novoa, J. J. Theoretical Study of the Electronic Structure of $[TCNQ]_2^{2-}$ (TCNQ = 7,7,8,8-Tetracyano-p-Quinodimethane) Dimers and Their Intradimer, Long, Multicenter Bond in Solution and the Solid State. *J. Phys. Chem. A* **2009**, *113*, 7124−7132.

(27) Koivisto, B. D.; Ichimura, A. S.; McDonald, R.; Lemaire, M. T.; Thompson, L. K.; Hicks, R. G. Intramolecular π-Dimerization in a 1,1'-Bis(Verdazyl)Ferrocene Diradical. *J. Am. Chem. Soc.* **2005**, *128*, 690−691.

(28) Boere, R. T.; French, C. L.; Oakley, R. T.; Cordes, A. W.; Privett, J. A. J.; Craig, S. L.; Graham, J. B. Preparation and Interconversion of Dithiatriazine Derivatives: Crystal, Molecular, and Electronic Structure of Bis(5-Phenyl-1,3,2,4,6-Dithiatriazine) $(PhCN_3S_2)_2$. *J. Am. Chem. Soc.* **2002**, *107*, 7710−7717.

(29) Boere, R. T.; Fait, J.; Larsen, K.; Yip, J. Preparation of 1,3,2,4,6-Dithiatriazines with Substituted Aryl Groups and the x-Ray Crystal Structure of the (4-Chlorophenyl)Dithiatriazine Dimer. *Inorg. Chem.* **2002**, *31*, 1417−1423.

(30) Beldjoudi, Y.; Nascimento, M. A.; Cho, Y. J.; Yu, H.; Aziz, H.; Tonouchi, D.; Eguchi, K.; Matsushita, M. M.; Awaga, K.; Osorio-Roman, I.; Constantinides, C. P.; Rawson, J. M. Multifunctional Dithiadiazolyl Radicals: Fluorescence, Electroluminescence, and Photoconducting Behavior in Pyren-1′-Yl-Dithiadiazolyl. *J. Am. Chem. Soc.* **2018**, *140*, 6260−6270.
(31) Cui, Z.; Lischka, H.; Beneberu, H. Z.; Kertesz, M. Double Pancake Bonds: Pushing the Limits of Strong π-π Stacking Interactions. *J. Am. Chem. Soc.* **2014**, *136*, 12958−12965.
(32) Haberhauer, G.; Gleiter, R. Double Pancake Versus Long Chalcogen-Chalcogen Bonds in Six-Membered C,N,S-Heterocycles. *Chem. Eur. J.* **2016**, *22*, 8646−8653.
(33) Boeré, R. T. Experimental and Computational Evidence for "Double Pancake Bonds": The Role of Dispersion-Corrected DFT Methods in Strongly Dimerized 5-Aryl-1λ^2,3λ^2-Dithia-2,4,6-Triazines. *ACS Omega* **2018**, *3*, 18170−18180.
(34) Tian, Y.-H.; Sumpter, B. G.; Du, S.; Huang, J. Pancake π-π Bonding Goes Double: Unexpected 4e/All-Sites Bonding in Boron- and Nitrogen-Doped Phenalenyls. *J. Phys. Chem. Lett.* **2015**, *6*, 2318−2325.
(35) Mou, Z.; Kertesz, M. Pancake Bond Orders of a Series of π-Stacked Triangulene Radicals. *Angew. Chem., Int. Ed.* **2017**, *56*, 10188−10191.
(36) Moilanen, J. O.; Day, B. M.; Pugh, T.; Layfield, R. A. Open-Shell Doublet Character in a Hexaazatrinaphthylene Trianion Complex. *Chem. Commun.* **2015**, *51*, 11478−11481.
(37) Gould, C. A.; Darago, L. E.; Gonzalez, M. I.; Demir, S.; Long, J. R. A Trinuclear Radical-Bridged Lanthanide Single-Molecule Magnet. *Angew. Chem., Int. Ed.* **2017**, *56*, 10103−10107.
(38) Zhang, P.; Luo, Q.-C.; Zhu, Z.; He, W.; Song, N.; Lv, J.; Wang, X.; Zhai, Q.-G.; Zheng, Y.-Z.; Tang, J. Radical-Bridged Heterometallic Single-Molecule Magnets Incorporating Four Lanthanoceniums. *Angew. Chem., Int. Ed.* **2023**, *62*, No. e202218540.
(39) Grindell, R.; Vieru, V.; Pugh, T.; Chibotaru, L. F.; Layfield, R. A. Magnetic Frustration in a Hexaazatrinaphthylene-Bridged Trimetallic Dysprosium Single-Molecule Magnet. *Dalton Trans.* **2016**, *45*, 16556−16560.
(40) Moilanen, J. O.; Chilton, N. F.; Day, B. M.; Pugh, T.; Layfield, R. A. Strong Exchange Coupling in a Trimetallic Radical-Bridged Cobalt(II)-Hexaazatrinaphthylene Complex. *Angew. Chem., Int. Ed.* **2016**, *55*, 5521−5525.
(41) Mantina, M.; Chamberlin, A. C.; Valero, R.; Cramer, C. J.; Truhlar, D. G. Consistent van Der Waals Radii for the Whole Main Group. *J. Phys. Chem. A* **2009**, *113*, 5806−5812.
(42) Noodleman, L. Valence Bond Description of Antiferromagnetic Coupling in Transition Metal Dimers. *J. Chem. Phys.* **1981**, *74*, 5737−5743.
(43) Jonkers, G.; de Lange, C. A.; Noodleman, L.; Baerends, E. J. Broken Symmetry Effects in the He(I) Valence Photoelectron Spectrum of $Se(CN)_2$. *Mol. Phys.* **1982**, *46*, 609−620.
(44) Noodleman, L.; Norman, J. G. Jr.; Osborne, J. H.; Aizman, A.; Case, D. A. Models for Ferredoxins: Electronic Structures of Iron-Sulfur Clusters with One, Two, and Four Iron Atoms. *J. Am. Chem. Soc.* **1985**, *107*, 3418−3426.
(45) Noodleman, L.; Davidson, E. R. Ligand Spin Polarization and Antiferromagnetic Coupling in Transition Metal Dimers. *Chem. Phys.* **1986**, *109*, 131−143.
(46) Moreira, I. d. P. R.; Illas, F. A Unified View of the Theoretical Description of Magnetic Coupling in Molecular Chemistry and Solid State Physics. *Phys. Chem. Chem. Phys.* **2006**, *8*, 1645−1659.
(47) Yamaguchi, K.; Fukui, H.; Fueno, T. Molecular Orbital (MO) Theory for Magnetically Interacting Organic Compounds. Ab-Initio MO Calculations of the Effective Exchange Integrals for Cyclophane-Type Carbene Dimers. *Chem. Lett.* **1986**, *15*, 625−628.
(48) Yamaguchi, K.; Tsunekawa, T.; Toyoda, Y.; Fueno, T. Ab Initio Molecular Orbital Calculations of Effective Exchange Integrals between Transition Metal Ions. *Chem. Phys. Lett.* **1988**, *143*, 371−376.
(49) Yamaguchi, K.; Jensen, F.; Dorigo, A.; Houk, K. N. A spin correction procedure for unrestricted Hartree-Fock and Møller-Plesset wavefunctions for singlet diradicals and polyradicals. *Chem. Phys. Lett.* **1988**, *149*, 537−542.
(50) Yanai, T.; Tew, D. P.; Handy, N. C. A New Hybrid Exchange-Correlation Functional Using the Coulomb-Attenuating Method (CAM-B3LYP). *Chem. Phys. Lett.* **2004**, *393*, 51−57.
(51) Becke, A. D. Density-Functional Exchange-Energy Approximation with Correct Asymptotic Behavior. *Phys. Rev. A* **1988**, *38*, 3098−3100.
(52) Lee, C.; Yang, W.; Parr, R. G. Development of the Colle-Salvetti Correlation-Energy Formula into a Functional of the Electron Density. *Phys. Rev. B: Condens. Matter Mater. Phys.* **1988**, *37*, 785−789.
(53) Goto, K.; Kubo, T.; Yamamoto, K.; Nakasuji, K.; Sato, K.; Shiomi, D.; Takui, T.; Kubota, M.; Kobayashi, T.; Yakusi, K.; Ouyang, J. A Stable Neutral Hydrocarbon Radical: Synthesis, Crystal Structure, and Physical Properties of 2,5,8-Tri-Tert-Butyl-Phenalenyl. *J. Am. Chem. Soc.* **1999**, *121*, 1619−1620.
(54) Morita, Y.; Aoki, T.; Fukui, K.; Nakazawa, S.; Tamaki, K.; Suzuki, S.; Fuyuhiro, A.; Yamamoto, K.; Sato, K.; Shiomi, D.; Naito, A.; Takui, T.; Nakasuji, K. A New Trend in Phenalenyl Chemistry: A Persistent Neutral Radical, 2,5,8-Tri-Tert-Butyl-1,3-Diazaphenalenyl, and the Excited Triplet State of the Gable Syn-Dimer in the Crystal of Column Motif. *Angew. Chem., Int. Ed.* **2002**, *41*, 1793−1796.
(55) Fukui, K.; Sato, K.; Shiomi, D.; Takui, T.; Itoh, K.; Gotoh, K.; Kubo, T.; Yamamoto, K.; Nakasuji, K.; Naito, A. Electronic Structure of a Stable Phenalenyl Radical in Crystalline State as Studied by SQUID Measurements, CW-ESR, and ^{13}C CP/MAS NMR Spectroscopy. *Synth. Met.* **1999**, *103*, 2257−2258.
(56) Mansikkamäki, A.; Tuononen, H. M. The Role of Orbital Symmetries in Enforcing Ferromagnetic Ground State in Mixed Radical Dimers. *J. Phys. Chem. Lett.* **2018**, *9*, 3624−3630.
(57) Kitaura, K.; Morokuma, K. A New Energy Decomposition Scheme for Molecular Interactions within the Hartree-Fock Approximation. *Int. J. Quantum Chem.* **1976**, *10*, 325−340.
(58) Ziegler, T.; Rauk, A. On the Calculation of Bonding Energies by the Hartree Fock Slater Method. *Theor. Chim. Acta* **1977**, *46*, 1−10.
(59) Ziegler, T.; Rauk, A. A Theoretical Study of the Ethylene-Metal Bond in Complexes between Copper(1+), Silver(1+), Gold(1+), Platinum(0) or Platinum(2+) and Ethylene, Based on the Hartree-Fock-Slater Transition-State Method. *Inorg. Chem.* **1979**, *18*, 1558−1565.
(60) Perdew, J. P.; Burke, K.; Ernzerhof, M. Generalized Gradient Approximation Made Simple. *Phys. Rev. Lett.* **1996**, *77*, 3865−3868.
(61) Perdew, J. P.; Burke, K.; Ernzerhof, M. Generalized Gradient Approximation Made Simple. *Phys. Rev. Lett.* **1997**, *78*, 1396.
(62) Ernzerhof, M.; Scuseria, G. E. Assessment of the Perdew-Burke-Ernzerhof Exchange-Correlation Functional. *J. Chem. Phys.* **1999**, *110*, 5029−5036.
(63) Adamo, C.; Barone, V. Toward Reliable Density Functional Methods without Adjustable Parameters: The PBE0Model. *J. Chem. Phys.* **1999**, *110*, 6158−6170.
(64) Barluzzi, L.; Chatelain, L.; Fadaei-Tirani, F.; Zivkovic, I.; Mazzanti, M. Facile N-Functionalization and Strong Magnetic Communication in a Diuranium(V) Bis-Nitride Complex. *Chem. Sci.* **2019**, *10*, 3543−3555.
(65) Kindra, D. R.; Evans, W. J. Magnetic Susceptibility of Uranium Complexes. *Chem. Rev.* **2014**, *114*, 8865−8882.
(66) Jin, Y.-Y.; Sun, S.-H.; Cui, Y.-W.; Zhu, Q.-Q.; Ji, L.-W.; Ren, Z.; Cao, G.-H. Bulk Superconductivity and Pauli Paramagnetism in Nearly Stoichiometric $CuCo_2S_4$. *Phys. Rev. Mater.* **2021**, *5*, 074804.
(67) Ji, X.; Xie, H.; Zhu, C.; Zou, Y.; Mu, A. U.; Al-Hashimi, M.; Dunbar, K. R.; Fang, L. Pauli Paramagnetism of Stable Analogues of Pernigraniline Salt Featuring Ladder-Type Constitution. *J. Am. Chem. Soc.* **2019**, *142*, 641−648.

https://doi.org/10.1021/jacs.3c13914
J. Am. Chem. Soc. 2024, 146, 4234−4241

(68) Matsubara, K.; Tsuzuku, T.; Sugihara, K. Electron Spin Resonance in Graphite. *Phys. Rev. B: Condens. Matter Mater. Phys.* **1991**, *44*, 11845−11851.
(69) Kausteklis, J.; Cevc, P.; Arčon, D.; Nasi, L.; Pontiroli, D.; Mazzani, M.; Riccò, M. Electron Paramagnetic Resonance Study of Nanostructured Graphite. *Phys. Rev. B: Condens. Matter Mater. Phys.* **2011**, *84*, 125406.
(70) Augustyniak-Jabłokow, M. A.; Tadyszak, K.; Maćkowiak, M.; Lijewski, S. ESR Study of Spin Relaxation in Graphene. *Chem. Phys. Lett.* **2013**, *557*, 118−122.
(71) Augustyniak-Jabłokow, M. A.; Tadyszak, K.; Maćkowiak, M.; Yablokov, Y. V. EPR Evidence of Antiferromagnetic Ordering in Single-Layer Graphene. *Phys. Status Solidi RRL* **2011**, *5*, 271−273.
(72) Kelly, A. G.; O'Suilleabhain, D.; Gabbett, C.; Coleman, J. N. The Electrical Conductivity of Solution-Processed Nanosheet Networks. *Nat. Rev. Mater.* **2022**, *7*, 217−234.
(73) Fratini, S.; Nikolka, M.; Salleo, A.; Schweicher, G.; Sirringhaus, H. Charge Transport in High-Mobility Conjugated Polymers and Molecular Semiconductors. *Nat. Mater.* **2020**, *19*, 491−502.
(74) Velho, M. F. G.; Silva, R. A. L.; Belo, D. The Quest for Single Component Molecular Metals within Neutral Transition Metal Complexes. *J. Mater. Chem. C* **2021**, *9*, 10591−10609.

https://doi.org/10.1021/jacs.3c13914
J. Am. Chem. Soc. 2024, 146, 4234−4241